Advances in Nano Research, *Vol. 11, No. 3 (2021) 271-280*
https://doi.org/10.12989/anr.2021.11.3.271

Strengthening effect of $Ti_3C_2T_x$ in copper matrix composites prepared by molecular-level and high-shear mixings and SPS

Lu Liu[1a], Guobing Ying*[1b], Dong Wen[2a], Cong Hu[1a], Chen Zhang[1a] and Cheng Wang[1b]

[1]*Department of Materials Science and Engineering, College of Mechanics and Materials, Hohai University, Nanjing, 211100, China*
[2]*Key Laboratory of Superlight Materials & Surface Technology (Harbin Engineering University), Ministry of Education, Harbin 150001, China*

(*Received August 15, 2020, Revised June 9, 2021, Accepted June 12, 2021*)

Abstract. MXene ($Ti_3C_2T_x$) reinforced copper matrix composites with weight fractions of MXene from 1 to 4 wt.% were fabricated based on molecular-level and high-shear mixings and spark plasma sintering (SPS) method. The mechanical properties of the composites with different weight fractions of MXene were studied, and X-ray photoelectron spectroscopy (XPS) was used to track the state of MXene in the composite preparation process. Chemical state and interface transitions would result in an interesting ductile-brittle transition phenomenon of the composite. The Vickers hardness and compressive strength of the composites prepared by the molecular-level mixing and high-shear mixing methods have been improved (the maxima are 44.9% and 41.8%, respectively), where the addition of 1wt.% MXene results in a tensile strength increase of 29.9%. The results show that molecular-level mixing and high-shear mixing methods are hopeful to be applied to produce many kinds of MXene composites.

Keywords: copper-based composites; mechanical properties; molecular-level and high-shear mixings; MXene $Ti_3C_2T_x$

1. Introduction

Two-dimensional (2D) nanomaterials, such as graphene (Kim *et al.* 2018, Low and Shon 2018), were widely used to improve the properties of copper matrix materials due to their unique properties in terms of high strength and elevated specific surface area (Butler *et al.* 2013, Kim *et al.* 2014, Li *et al.* 2014, Wang *et al.* 2015a, Zhang and Zhan 2016a, b). Kim *et al*. (2014) prepared graphene/Cu composite by ball milling and high-ratio differential speed rolling techniques, which effectively improved the strength of the material. While the combination of mechanical property and conductivity of graphene is in general difficult to surpass, the complexity and limited improvement of uniformity have energized efforts, especially in the 2D community, to find alternatives. MXene belongs to a family of 2D transition metal carbides or carbonitrides, with a chemical formula of $M_{n+1}X_nT_z$, where M is an early transition metal, X corresponds to C and/or N, T stands for surface-terminating functional groups (e.g., F^-, OH^-, O^{2-}), and n = 1, 2, 3 or 4 (Naguib *et al.* 2011, Deysher *et al.* 2019). Most terminations of MXene obtained through chemical etching consist of –OH and –O groups (Naguib *et al.* 2012, Yu *et al.* 2014). MXene possesses a unique 2D layered structure and large specific surface area combined with good conductivity, relevant stability, and superior magnetic/mechanical properties. Films made of MXene colloidal solutions are typically quite conductive (Ying *et al.* 2017), MXene also has excellent catalytic properties (Zhao *et al.* 2018). However, to date, by far the most studied MXene composites remain the polymer-matrix materials (Carey *et al.* 2019, Wang *et al.* 2019, Zhang *et al.* 2016).

A well-dispersed state ensures the availability of maximum surface area of filler and the properties of the whole nanocomposite. Therefore, nano-fillers should be incorporated into the matrices through different methods to achieve good interface bonding and uniform distribution. Different from the traditional preparation method, the molecular-level mixing method is an ideal choice for preparing copper-based composite materials (Cha *et al.* 2005). The copper salt solution can be easily reduced to copper oxide or copper, which is the premise of the molecular-level mixing method (Kobayashi *et al.* 2017). Molecular-level mixing method, that is, after the nanofiller is mixed with the copper salt solution, the nanofiller is uniformly dispersed in the precipitate through heating and evaporation or chemical reaction, and then the mixture powder with uniform filler dispersion is obtained by reducing the copper oxide. Hwang *et al.* (2013) demonstrated that molecular-level mixing could be used to produced reduced graphene oxide reinforced copper matrix composites with a tensile strength of 284 MPa. Zhang and Zhan (2016a) prepared the copper matrix composites reinforced with graphene nanoplatelets, nickel-plated graphene nanoplatelets, and reduced graphene oxide by the molecular-level mixing process. However, the molecular-

*Corresponding author, Ph.D., Professor,
E-mail: yinggb2010@126.com; yinggb001@hhu.edu.cn
[a] Student
[b] Ph.D., Professor

ISSN: 2287-237X (Print), 2287-2388 (Online)

level mixing method can improve the dispersion of nanofillers, but it cannot solve the problem of agglomeration. High-shear mixing can produce a high-shear force on the materials in liquids by the rotor-stator mixer and has been widely used to handle processes such as emulsification and homogenization (Atiemo-Obeng and Calabrese, 2004). Wang *et al.* (2015a) used the high-shear mixing based on the molecular-level mixing method to significantly improve the dispersion of filler in the matrix and prepared the reduced graphene oxide/Cu composite with the maximum compressive yield strength of 501.3 MPa. Si *et al.* (2018) compounded multiple layers of MXene with copper through the molecular-level mixing method, which significantly improved the tribological properties of the composite.

In this paper, the rotor-stator mixer based on the molecular-level mixing method was used to introduce the high-shear mixing method, which could make the filler ($Ti_3C_2T_x$) distributed in the composite more uniformity. MXene ($Ti_3C_2T_x$) reinforced copper matrix composites were prepared using SPS. And XPS was used to track the state of MXene during the preparation process. The tendency and mechanism of MXene to enhance the mechanical properties of copper were discussed.

2. Experimental

2.1 Fabrication of composites

Comprehensive details regarding all materials and preparation of Ti_3AlC_2 are provided in our earlier papers (Su *et al.* 2018, Zhang *et al.* 2019). The preparation process of MXene/Cu composites is displayed in Fig. 1. The Ti_3AlC_2 powders (1g) were placed into a mixture containing 1 g lithium fluoride (LiF, 99 wt. % purity, Shanghai Macklin Biochemical Co., Ltd., Shanghai, China) and 10 ml hydrochloric acid at 12M (HCl AR, Shanghai Lingfeng Chemical Reagent Co., Shanghai, China) at 35°C for 24 h to form a suspension with multilayered $Ti_3C_2T_x$ (M-$Ti_3C_2T_x$) flakes. The M-$Ti_3C_2T_x$ flakes were repeatedly washed with deionized water (resistivity > 18 MΩ·cm) and centrifuged at 3500 rpm (5 min for each cycle). The supernatant was then decanted, and the process was repeated until the pH value was greater than 6. The washing process was carried out at least 10 times, and the obtained powders were mixed with 25ml deionized water and sonicated for 1h at room temperature under bubbling Ar gas then centrifuged for 1h at 3500 rpm. The resulting supernatant colloidal solution mostly contained delaminates with single 2D $Ti_3C_2T_x$ flakes.

A typical molecular-level mixing method route of the composite powder of MXene and copper was given as follows. One hundred grams of copper sulfate pentahydrate ($CuSO_4 \cdot 5H_2O$, 99 wt. % purity, Sinopharm Chemical Reagent limited corporation, Shanghai, China), 40g sodium hydroxide (NaOH, AR, Sinopharm Chemical Reagent limited corporation, Shanghai, China) and 160g glucose ($C_6H_{12}O_6 \cdot H_2O$, AR, Sinopharm Chemical Reagent limited corporation, Shanghai, China) were dissolved in 400ml, 200 ml and 400 ml deionized water, respectively. Supernatant S-$Ti_3C_2T_x$ colloidal solutions were added to glucose solution and dispersed by ultrasonic, and then the mixture was quickly mixed with copper sulfate solution and sodium hydroxide solution at 60°C for 3 h, and the following reaction occurred (Fehling 1849, Liu *et al.* 2015):

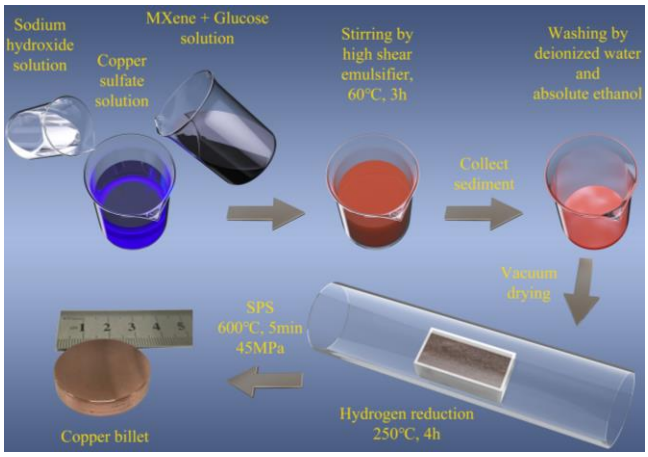

Fig. 1 Diagrammatic sketch of the preparation process of Cu/MXene composites

$$RCHO + 2Cu^{2+} + 5OH^- \rightarrow RCOO^- + Cu_2O + 3H_2O$$

where *RCHO* is an organic substance containing aldehyde groups, such as glucose.

High-shear mixing was introduced into this process of molecular-level mixing. In the process of reducing Cu^{2+} by glucose, the rotor-stator mixer (JRJ300-SH, Shanghai Huxi industry Co., LTD) was used to provide high shear emulsified mixed liquid at 6000 rpm rotating speed to make the dispersion of MXene more uniform. After the molecular-level and high-shear mixings, the mixture was repeatedly washed with deionized water and absolute ethanol until the pH value was close to neutral. Then a precipitate can be obtained by a centrifuge at 3500 rpm for 3 min. After vacuum drying, the precipitated powders were reduced at 250°C for 4h under an atmospheric pressure of hydrogen.

The reduced powders were then vacuum sintered by spark plasma sintering (SPS) at 600°C for 5 min and under a pressure of 40 MPa. The final sizes of as-fabricated MXene/Cu composites were 30 mm in diameter and 5 mm in thickness. Finally, four groups of samples with MXene content of 0, 1 wt.%, 2 wt.% and 4 wt.% were fabricated and named as T0, T1, T2, and T4, respectively.

2.2 Characterization

The chemical states of $Ti_3C_2T_x$ MXene were studied by XPS (Thermo ESCALAB 250XI, USA) equipped with a 400 μm monochromated Al Kα X-ray beam source, and used for irradiation of sample surface at a base pressure of 1×10^{-8} mbar. The photoelectrons were collected using a 180° hemispherical electron energy analyzer. The samples were analyzed at a 45° take-off angle between the sample surface and path to the analyzer. High-resolution spectra of

Ti 2p, C 1s and O 1s were collected at a pass energy of 50 eV with a step size of 0.05 eV. The fitting of high-resolution peaks of Ti 2p, C 1s and O 1s was performed by using XPSPEAK Version 4.1. Before quantification and peak fitting, background contributions were subtracted by using a Shirley function. For 2p3/2 and 2p1/2 components, the intensity ratios of the peaks were kept at 2:1. The phase composition was determined by X-ray diffraction (XRD, Bruker D8 advance, GER) with Cu Kα radiation source operating at 50 kV and 150 mA. The fracture surfaces of specimens after mechanical testing were observed at 5 kV by scanning electron microscopy (SEM, JEOL JSM-7600F, JPN). Moreover, an energy-dispersive X-ray spectrometer (EDS, Oxford INCA X-Act, GBR) was utilized to analyze the elements of the samples.

Tensile tests were performed at room temperature using an Instron 3367 mechanical testing machine (Instron, USA) following ISO 6892-1:2009, and standard dumbbell-shaped specimens (26.0 mm long × 6.0 mm wide × 2.0 mm thick) with a length of the narrow region of 10 mm were prepared for tensile testing at a rate of 0.6 mm min^{-1}. Compressive tests were performed using an Instron 3367 mechanical testing machine with a crosshead speed of 0.5 mm/min, and the samples had a cylindrical disk shape of 3 mm height and 3 mm diameter (Cui *et al.* 2014, Wang *et al.* 2015a, b). The loading direction is parallel to the pressing direction of SPS. The density measurement adopted the Archimedes drainage method. Vickers hardness was measured by using HX-1000TM/LCD hardness tester (Shanghai Optical Instrument Factory, CHN). The load was 0.1 Kgf, and the holding time was 25 s for each measurement. Three samples were tested from each sintered billet to minimize the error.

3. Results and discussion

The T4 component with the largest addition of MXene was selected for XRD characterization. The XRD patterns of MXene, T4 precipitate powders, T4 composite powders after reduction by H_2, and T4 composite sintered by SPS are shown in Fig. 2. Typical MXene $Ti_3C_2T_x$ diffractogram in that the (00 2) peak is at 2θ of 6.32°. However, The peak signal of MXene can not be detected in the precipitate powder, which is obtained after molecular-level mixing, high-shear mixing and washing, which is because the X-ray diffraction signals of the cuprous oxide (Cu_2O) are too strong. In addition, the 2D surface of the MXene sheet layer is covered by Cu_2O (as shown in Fig. 3), resulting in a reduction of the characteristic surface, which can also cause the reduction or even disappearance of the characteristic peaks. Similar phenomena are common in graphene/copper composites (Wang *et al.* 2015, Kim *et al.* 2014, Zhao *et al.* 2014) and MXene/polymer composites (Liu *et al.* 2021). After reduction by H_2, the Cu_2O is phase transition to pure copper. Besides, weak diffraction peaks of titanium dioxide (TiO_2) are found, indicating that there is oxidation on the MXene $Ti_3C_2T_x$, which is probably due to the fact that water is produced in the hydrogen reduction makes MXene more easily to be oxidized. After being sintered into a billet of composite by SPS, there is no obvious phase change in the processing.

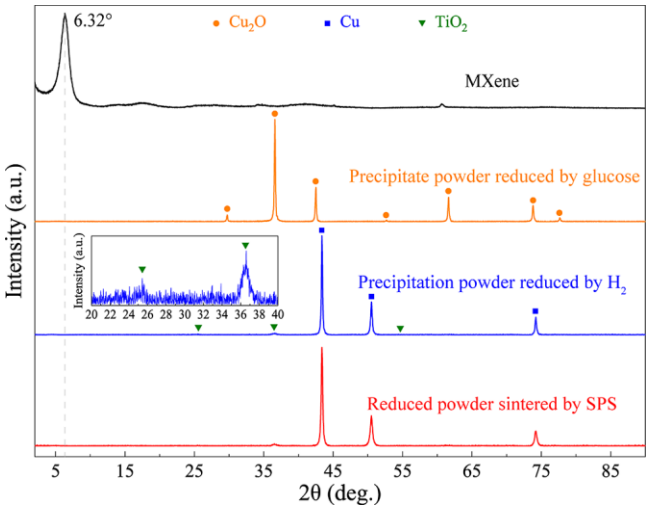

Fig. 2 XRD patterns of the MXene, T4 precipitate powders, T4 composite powders after reduction by H_2, and T4 composite sintered by SPS

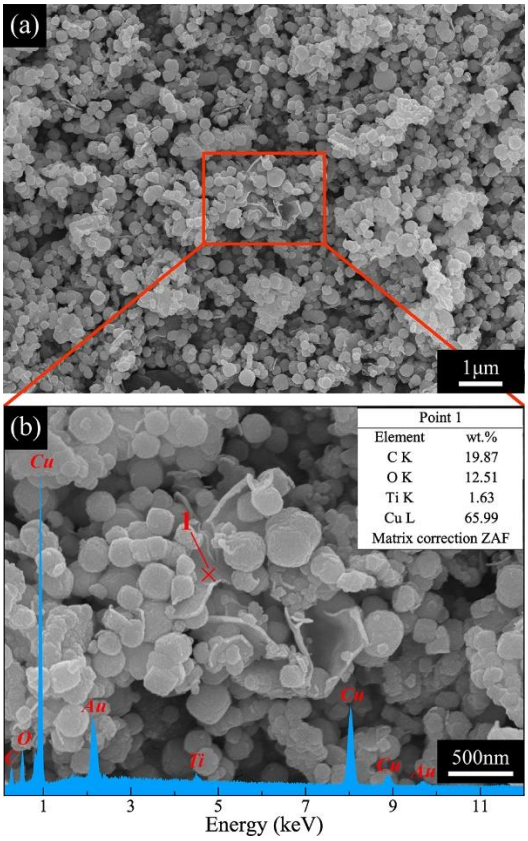

Fig. 3 (a) SEM micrograph of precipitate powders after vacuum dring and (b) EDS corresponding to the marked points

Fig. 3 shows the typical SEM micrographs of precipitate powders after vacuum drying. MXene could be identified from the powders based on their unique flake appearance and the Fig. 3b EDS result. Most MXene sheets are utterly or partially covered by Cu_2O particles and evenly dispersed in the Cu_2O powders. The average particle size of the generated Cu_2O particles is ~200 nm, and the maximum particle size does not exceed 500 nm.

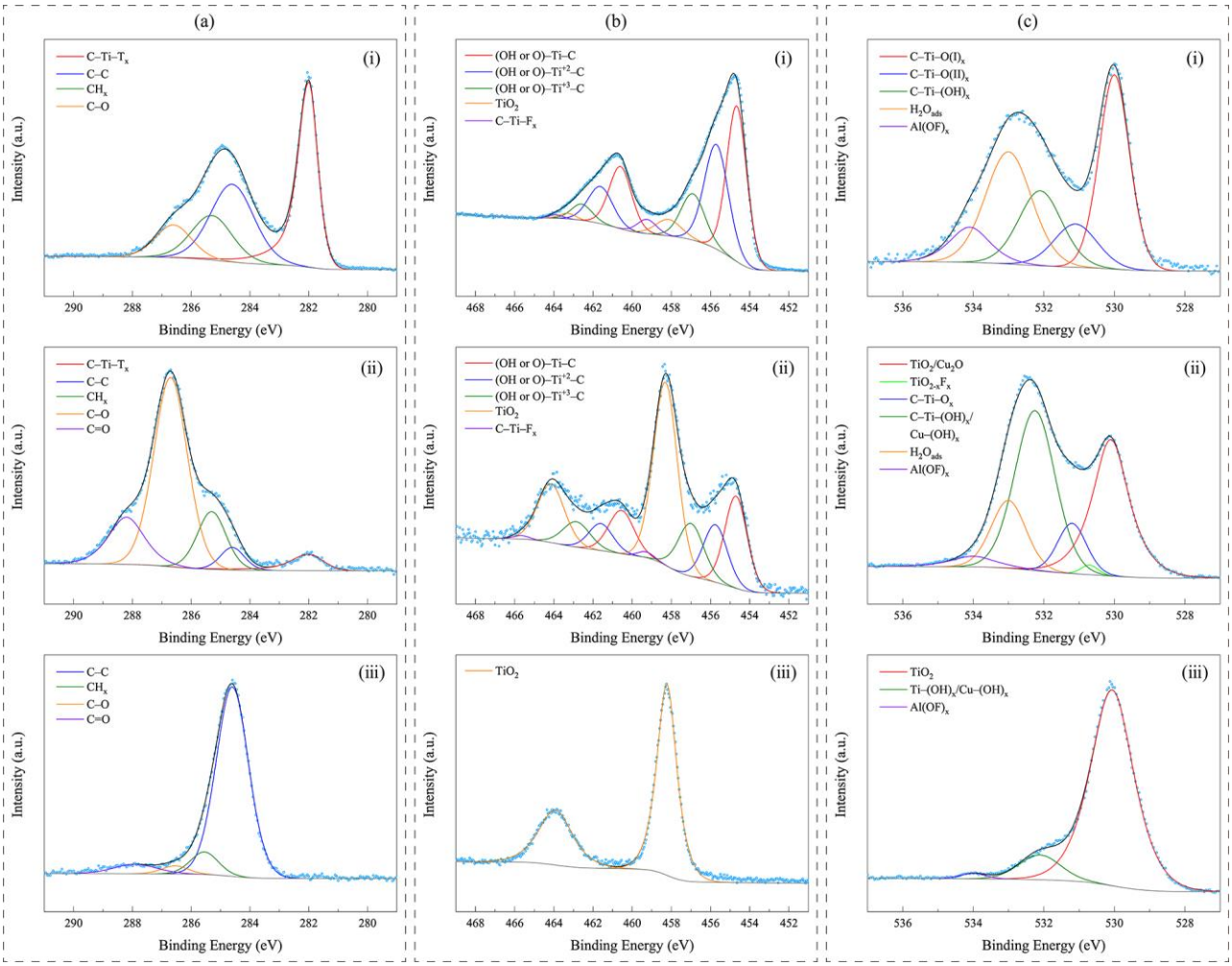

Fig. 4 High-resolution XPS spectra of (a) C 1s, (b) Ti 2p, and (c) O 1s of (i) MXene, (ii) precipitate powder and (iii) hydrogen reduced powder

To know the state of MXene $Ti_3C_2T_x$ in different periods of the preparation process adopted in this work, XPS was used to test MXene, precipitate powder and hydrogen reduction powder. For better understanding, T4, with the most MXene additions, was chosen for characterization. The resulting C 1s, Ti 2p and O 1s high-resolution XPS spectra are illustrated in Fig. 4. Fig. 4(a) exhibits high-resolution XPS spectra of C 1s region with deconvoluted peaks of C–Ti–T_x (282.0 eV), C–C (284.6 eV), CH_x (285.3 eV), C–O (286.6 eV) and COO (288.2 eV) bonds(Cao *et al.* 2017, Halim *et al.* 2014, 2018, Liu *et al.* 2019, Shah *et al.* 2016). Compared to the C1s spectrum of MXene (Fig. 4(a)(i)), the peak intensity of C–C, CH_x, C–O and COO significantly increase, as shown in Fig. 4(a)(ii). For the powder reduced by hydrogen, the peak intensities of CH_x, C–O and COO decreased, and the peak intensity of C–Ti–T_x disappeared, as shown in Fig. 4(a)(iii). Ti 2p XPS pattern (Fig. 4(b)) exhibits the existence of five peaks at 454.7, 455.7, 457.0, 458.2 and 459.0 eV, which are ascribed to (OH, or O)–Ti–C, (OH, or O)–Ti^{2+}–C, (OH, or O)–Ti^{3+}–C, TiO_2 and C–Ti–F_x, respectively(Cao *et al.* 2017, Halim *et al.* 2018, Shah *et al.* 2016, 2018). Compared with the Ti 2p spectrum of MXene (Fig. 4b (i)), the peak intensity of the TiO_2 bond in the precipitate in Fig. 4(b)(ii) increases significantly, and only the peak of the TiO_2 bond remained in the hydrogen-reduced powder, as shown in Fig. 4(b)(iii). The O 1s peaks of MXene are resolved into five component peaks identified as C–Ti–$O(I)_x$ (530.0 eV), C–Ti–$O(II)_x$ (531.1 eV), C–Ti–$(OH)_x$ (532.1 eV), H_2O_{ads} (533.0 eV), and $Al(OF)_x$ (534.0 eV)(Cao *et al.* 2017, Halim *et al.* 2018, Shah *et al.* 2016), as shown in Fig. 4(c)(i). There's new peak intensity of the $TiO_{2-x}F_x$ (530.6 eV) (Halim *et al.* 2018) bond in the precipitate in Fig. 4(c)(ii). It should be noted that the lattice oxygen peak position fitting for mixed metal oxides is relatively difficult because the binding energies are very close and are stacked together. Similarly, free oxygen such as hydroxyl groups adsorbed on the surface is difficult to distinguish between specific chemical bonds. Hence the peaks at 530.0 and 532.1 eV are expressed as TiO_2/Cu_2O and C–Ti–$(OH)_x$/Cu–$(OH)_x$, respectively (Aguirre *et al.* 2017, Sun *et al.* 2016, Xu *et al.* 2008). The O1s of the hydrogen reduction powder shows that the content of free oxygen decreases greatly, and the absorbed water even disappears, as shown in Fig. 4(c)(iii). According to the results of XPS, the state changes of MXene during the preparation of composites can be ascertained, which

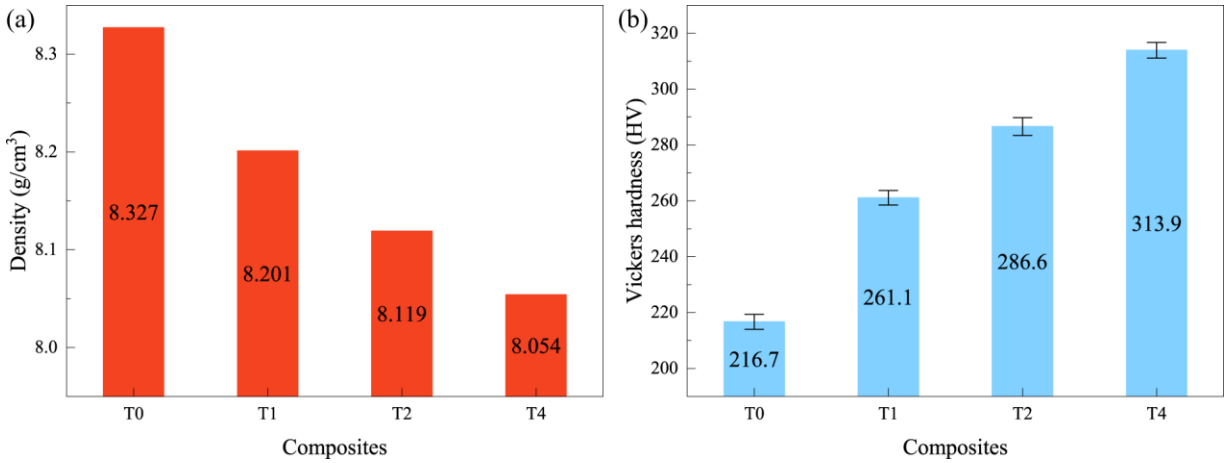

Fig. 5 (a) Density and (b) Vickers hardness of copper matrix composites

Table 1 The theoretical density, relative density and porosity calculation results of copper matrix composites with different reinforcement contents

Samples	Density (g·cm^{-3})	Theoretical density (g·cm^{-3})	Relative density (%)	Porosity (%)
T0	8.327	8.960	92.94	7.06
T1	8.201	8.826	92.92	7.08
T2	8.119	8.696	93.36	6.64
T4	8.054	8.447	95.35	4.65

which are summarized as follows: First, MXene was partially oxidized during the process of generating cuprous oxide, and the surface of the powder adsorbs organic substances generated in the synthesis process, such as gluconic acid; then in the process of the precipitate washing by absolute ethanol, a large number of hydroxyl groups were introduced, but the dehydration reduced the content of adsorbed water slightly; finally, after the reduction of the precipitate powder by hydrogen, MXene had been completely oxidized to TiO_2, and most of the attached organic matter and adsorbed water were removed during the reduction process. The oxidation of MXene was mainly attributed to the effect of some by-products in the hydrogen reduction process under heated. For example, $Ti_3C_2T_x$ can be oxidized by H_2O at 180°C (Feng *et al.* 2019, Li *et al.* 2020). It can be seen from the XPS results that the mixture is contaminated with organic matter, so during the reduction process, products other than H_2O were generated, such as carbon dioxide (CO_2). According to the literature (Naguib *et al.* 2014), $Ti_3C_2T_x$ can be oxidized by CO_2 at 150°C. In addition, volatile organic compounds were all possible sources of active oxygen.

Figs. 5(a) and 5(b) exhibit the density and Vickers hardness of copper matrix composites at different filler $Ti_3C_2T_x$ loadings, respectively. It can be found from Fig. 5a that the densities of the composites decrease wiht an increase in the number of MXene. The densities of T0, T1, T2 and T4 are 8.327 g·cm^{-3}, 8.201 g·cm^{-3}, 8.119 g·cm^{-3} and 8.054 g·cm^{-3}, respectively. Since the MXene in the composites has been oxidized, the theoretical density, relative density and porosity of the copper-matrix composites are calculated based on the TiO_2 density, and the results are shown in Table 1. In addition to the density of MXene (5.2 g·cm^{-3}) (Eom *et al.* 2020) and TiO_2 (4.23 g·cm^{-3}) (Lide, 2000) being significantly smaller than that of Cu (8.96 g·cm^{-3}), this phenomenon is also related to the introduction of densification caused by excessive filler addition. The introduction of reinforcement can fill the gaps between copper crystal grains, resulting in an increase in the relative density of the composite material and a decrease in porosity.

As shown in Fig. 5(b), the Vickers hardnesses of the composites also continues to increase as the addition amounts of MXene increase. The Vickers hardnesses of T1, T2 and T4 composites are 261.1, 296.6 and 313.9, respectively. Compared to T0 pure copper, the Vickers hardness of T4 composite increases by 44.9%. The hardness is improved with increasing the MXene concentration, which is a typical response for such composites that contain flaked shape particles such as graphene (Khamaj *et al.* 2021, Sadoun *et al.* 2021). The improved hardness is due to the presence of the reinforcement at the grain boundaries, which reduces the deformation between grains and hence reduces the plastic deformation of the composite. Additionally, the precipitated reinforcement inside the Cu grains embeds the movement of dislocation, which reduces the plastic deformation as well (Wagih 2015, Wagih and Fathy 2016, Eltaher *et al.* 2020, Sadoun *et al.* 2020). The reduction of the plastic deformation reduces the indentation depth of the indenter inside the samples (since the hardness test is an indentation test) and the hardness is inversely proportional to the indentation depth. So, the hardness is improved.

The mechanical properties of the composites were

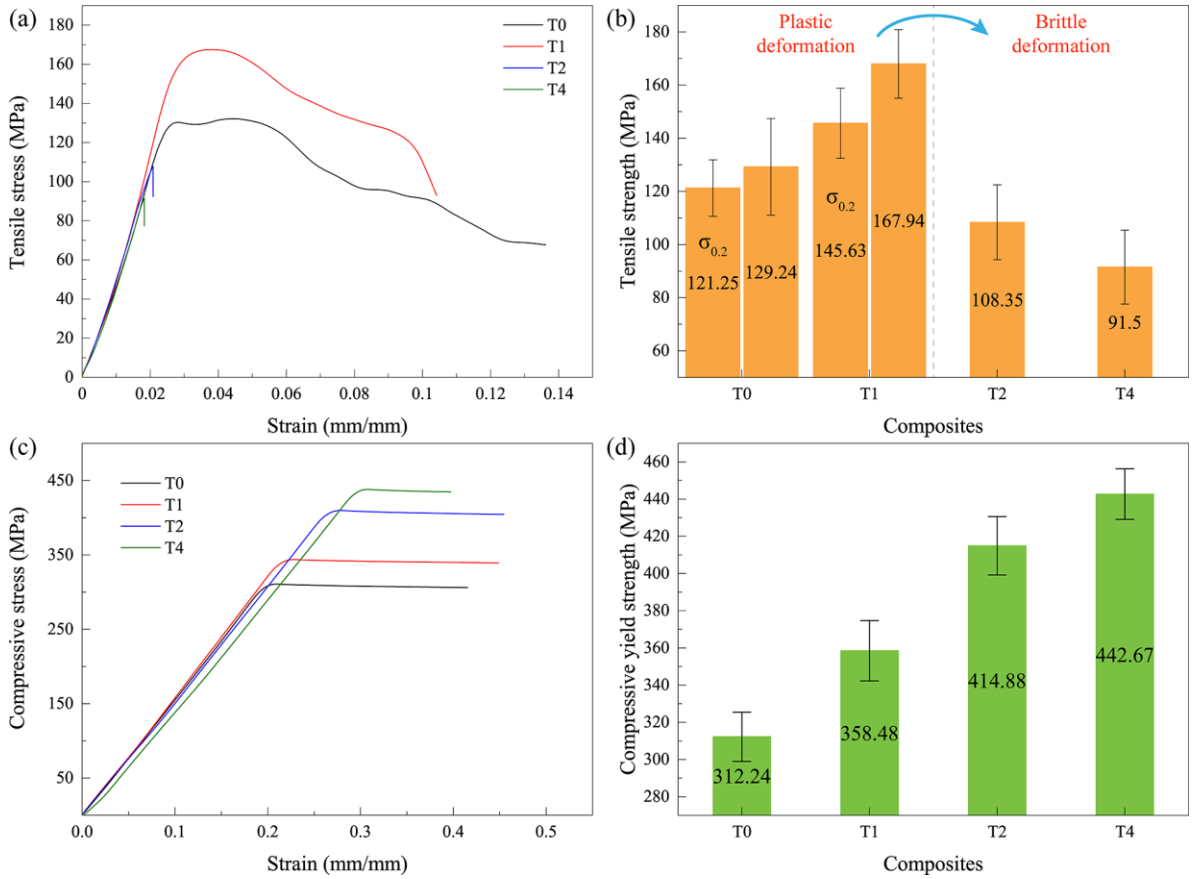

Fig. 6 (a) Typical tensile stress-strain curves, (b) tensile strength, (c) compressive stress-strain curves and (d) compressive strength of copper matrix composites

characterized using tensile and compressive tests. Fig. 6(a) shows the typical tensile stress-strain curves of copper matrix composites. The strains at the maximum stresses of T0, T1, T2, and T4 are 4.6%, 3.7%, 2.1%, and 1.8%, respectively; And the strain of the composite is inversely proportional to the amount of reinforcement added. It is found that the T0 and T1 exhibit the plastic tensile curves, while the T2 and T4 are changed to brittle tensile curves. The change of the tensile curve reflects that the introduction of different fillers can cause a ductile-brittle transition. When the addition amount of the reinforcement is appropriate (such as 1wt.%), the dispersion strengthening of the second phase plays a major role, and the composite still exhibits toughness while the mechanical properties of the composite are enhanced; When the addition of the reinforcement continues to increase, there are more weak interfaces between the copper grains due to the weaker Van der Waals force combination between TiO_2 and Cu, and the effect of dispersion strengthening does not occupy the main role, the composite exhibits brittleness while the mechanical properties deteriorate. In addition, In the tensile test, the weak interface acts as the initiator of cracks, accelerating the fracture process of the specimen and reducing the deformation before the specimen fails (Wagih *et al.* 2018). Fig. 6(b) illustrates the tensile strengths of copper matrix composites with MXene contents. The tensile property of T1 reaches the maximum value, and the tensile strength (σ_b = 167.94 MPa) is increased by 29.9% compared with T0 (σ_b = 129.24 MPa). And the yield strengths $\sigma_{0.2}$ of T0 and T1 composites are 121.25 MPa and 145.63 MPa, respectively. The tensile strengths of T2 and T4 composites are 16.2% (σ_b = 108.35 MPa) and 29.2% (σ_b = 91.50 MPa), respectively, which decrease with the increase of filler content and are lower than that of T0.

Figs. 6(c) and 6(d) show the typical compressive stress-strain curves and yield strengths of the copper matrix composites, respectively. The compressive yield strength continues to increase as the amount increase of the filler $Ti_3C_2T_x$. Compared with T0 (312.24 MPa), T4 (442.67 MPa) has the most significant increase in compressive strength, which is 41.8% higher than that of T0. The Vickers hardness, tensile strength, and compressive strength of the copper matrix composites compared to reported literatures' values are shown in Table 2.

Obviously, the introduction of MXene ($Ti_3C_2T_x$) has a significant strengthening effect on the copper matrix. The strengthening effect of $Ti_3C_2T_x$ on the tensile strength is a little lower than that of the graphene nanoplatelets (Zhang and Zhan 2016a), nickel-plated graphene nanoplatelets (Zhang and Zhan 2016a), reduced graphene oxide (Hwang *et al.* 2013, Zhang and Zhan 2016b), multi-layer graphene (Kim *et al.* 2014) or Graphene nanoplatelets (Zhao and Wang 2014). But the effect of $Ti_3C_2T_x$ on the compressive strength is much higher than those of carbon nanotubes (Cha *et al.* 2005), carbon nanosheet (Wang *et al.* 2015b) and reduced graphene oxide (Wang *et al.* 2015a). Moreover,

Table 2 Comparison of the Vickers hardness, tensile strength, and compressive strength of copper matrix and the relative increments after incorporation of various nanofillers

Reinforcement filler content	Gain in Vickers hardness [%] (matrix)	Gain in tensile strength [%] (matrix [MPa])	Gain in compressive strength [%] (matrix [MPa])	Reinforcement filler and References
1 wt.%	20.5 (216.7)	29.9 (129.24)	14.8 (312.24)	
2 wt.%	32.3 (216.7)	-16.2 (129.24)	32.9 (312.24)	$Ti_3C_2T_x$, this work
4 wt.%	44.9 (216.7)	-29.2 (129.24)	41.8 (312.24)	
0.5 vol.%	-	13.3 (226)	-	Graphene nanoplatelets (Zhang and Zhan 2016a)
0.5 vol.%	-	24.3 (226)	-	Nickel-plated graphene nanoplatelets (Zhang and Zhan 2016a)
0.5 vol.%	-	23.0 (226)	-	Reduced graphene oxide (Zhang and Zhan 2016b)
2.5 vol.%	-	30 (255)	-	Reduced graphene oxide (Hwang *et al.* 2013)
0.5 vol.%	-	4.5 (384.2)	-	Multi-layer graphene [1] (Kim *et al.* 2014)
1 vol.%	-	10.7 (384.2)	-	
5 vol.%	-		230 (~156)	Carbon nanotubes (Cha *et al.* 2005)
10 vol.%	-		300 (~156)	
2.5 vol.%	-	-	170 (275)	Carbon nanosheet (Wang *et al.* 2015b)
2.4 vol.%	-	-	300 (~167.1)	Reduced graphene oxide (Wang *et al.* 2015a)
1.3 wt.%	-	107% (234)	-	Graphene nanoplatelets [2] (Zhao and Wang 2014)

[1] High-ratio differential speed rolling; [2] Electroless plating process

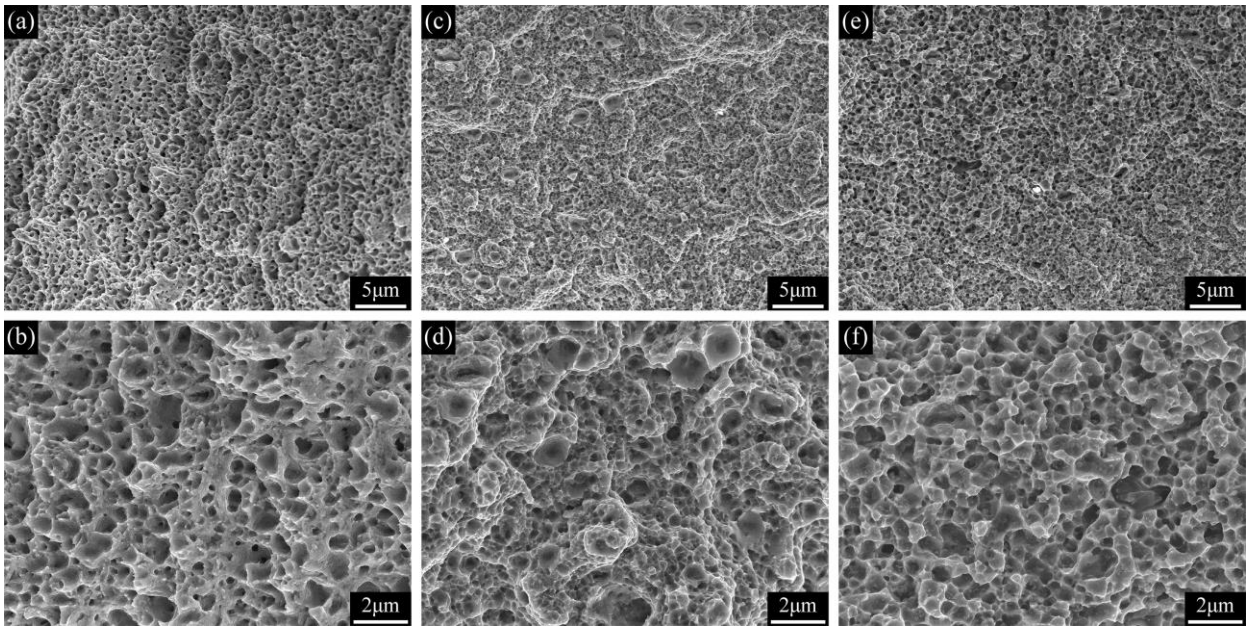

Fig. 7 SEM images of tensile fracture surfaces of (a, b) T0 (c, d) T1, and (e, f) T4 composites

the toughening effect only can be found when the mass fraction of MXene is no more than 1 wt.%. It is very interesting that there is a ductile-brittle transition in the copper matrix composites. In this case, MXene ($Ti_3C_2T_x$) and its resultant oxide, i.e. TiO_2, should be considered at the same time. It is worth noting that the XPS shows the different chemical states of the $Ti_3C_2T_x$ and TiO_2. In order to better understanding the mechanism of the ductile-brittle transition phenomenon, the microscopic morphologies of the tensile fracture of T0, T1, and T4 composites are shown in Figs. 7(a)-7(f). The uniform fracture features with dimples indicate that the molecular-level and high-shear mixings conducted in the preparation process can result in the uniform dispersion feature of the filter and matrix. At

this time, dispersion strengthening is the main strengthening and toughening mechanism. The main morphological characteristics of the fracture of the T0 specimen (see Figs. 7(a) and 7(b)) are the equiaxed dimples after uniaxial stretching, where the dimples are evenly distributed and uniform in size. It is a typical ductile fracture feature, indicating that the material has good toughness. The dimples' size of T1 fracture becomes nonuniform, and the dimples' depth becomes shallow, as shown in Figs. 7(c) and 7(d). This reveals that the packing bears part of the load transmitted by the matrix. And the step-like drop in Fig. 7(c) shows that the filler deflects the crack when the damage occurs. Figs. 7(e) and 7(f) are the tensile fracture morphologies of the T4 composite. It can be clearly observed that the depths of dimples become very shallow, indicating that the plasticity of the material is further reduced. This is consistent with the tensile strength test results. Besides, some large deep pits can be observed, indicating the occurrence of defects. According to the XPS and XRD results, together with that of the mechanical behavior, there should be the action of the filler TiO_2. As is known to all, the interface strength between the metal oxide TiO_2 and the metal matrix is poor.

Although the molecular-level and high-shear mixings can result in the uniform dispersion feature of the filter, there's no use to change the bonding between the resultant TiO_2 and matrix copper. With more MXene content in the composite, more content and chance of the resultant oxide TiO_2 could be found. Due to the poor wettability of metal oxide and metal, with the continuous increase of filler, too many weak bonding interfaces are introduced into the composite, which is the main reason for the decrease of tensile strength and lower than T0. Unlike the metal bond in the matrix, the ion bond in the filler TiO_2 is difficult to slip. Therefore, when the composite was loaded, the filler TiO_2 prevented the slip of metal grains or dislocations, which made it difficult to deform and improved the compressive strength.

4. Conclusions

The use of molecular-level mixing and high-shear mixing can ensure that MXene is uniformly dispersed in the copper matrix. However, the process of hydrogen reduction of cuprous oxide particles could cause the resultant oxidation of MXene into TiO_2. The addition of fillers reduces the density of the composite but increases the Vickers hardness and compressive strength of the composites. When the amount of MXene addition is 4 wt.%, Vickers hardness and compressive strength can be increased by 44.9% and 41.8%, respectively. As MXene was oxidized, too many fillers had a negative optimization in terms of tensile properties. Chemical state and interface transitions are two main mechanisms for the negative phenomenon. However, a reasonable amount of addition (such as 1 wt.%) can still increase the tensile strength by 29.9%. The molecular-level mixing and high-shear mixing methods are hopeful to be applied to produce many kinds of MXene based composites, and promising perspectives are opened up by integrating high-shear mixing in the process of composite production, but still need to overcome the oxidation problem of MXene.

Acknowledgments

The authors greatly acknowledge the financial support from the National Natural Science Foundation of China (Grant No. 11872171) and Fundamental Research Funds for the Central Universities (Grant No. B200202117).

References

Aguirre, M.E., Zhou, R., Eugene, A.J., Guzman, M.I. and Grela, M.A. (2017), "Cu_2O/TiO_2 heterostructures for CO_2 reduction through a direct Z-scheme: Protecting Cu_2O from photocorrosion", *Appl. Catal. B Environ.*, **217**, 485-493. https://doi.org/10.1016/j.apcatb.2017.05.058

Atiemo-Obeng, V.A. and Calabrese, R.V. (2004), *Rotor-Stator Mixing Devices* in *Handbook of Industrial Mixing: Science and Practice*, 479-505, John Wiley & Sons, Inc., New Jersey, U.S.A.

Butler, S.Z., Hollen, S.M., Cao, L., Cui, Y., Gupta, J.A., Gutiérrez, H.R., Heinz, T.F., Hong, S.S., Huang, J. and Ismach, A.F. (2013), "Progress, challenges, and opportunities in two-dimensional materials beyond graphene.", *ACS Nano*, **7**(4), 2898-2926. https://doi.org/10.1021/nn400280c.

Cao, M., Wang, F., Lei, W., Wu, W., Lv, W. and Zhu, J. (2017), "Room temperature oxidation of Ti_3C_2 MXene for supercapacitor electrodes", *J. Electrochem. Soc.*, **164**(14), A3933-A3942. https://doi.org/10.1149/2.1541714jes.

Cao, Y., Deng, Q., Liu, Z., Shen, D., Wang, T., Huang, Q., Du, S., Jiang, N., Lin, C. and Yu, J. (2017), "Enhanced thermal properties of poly(vinylidene fluoride) composites with ultrathin nanosheets of MXene", *RSC Adv.*, **7**(33), 20494-20501. https://doi.org/10.1039/C7RA00184C

Carey, M.S., Sokol, M., Palmese, G.R. and Barsoum, M.W. (2019), "Water transport and thermomechanical properties of $Ti_3C_2T_z$ MXene epoxy nanocomposites", *ACS Appl. Mater. Interfac.*, **11**(42), 39143-39149. https://doi.org/10.1021/acsami.9b11448.

Cha, S.I., Kim, K.T., Arshad, S.N., Mo, C.B. and Hong, S.H. (2005), "Extraordinary strengthening effect of carbon nanotubes in metal-matrix nanocomposites processed by molecular-level mixing", *Adv. Mater.*, **17**(11), 1377-1381. https://doi.org/10.1002/adma.200401933.

Cui, Y., Wang, L., Li, B., Cao, G. and Fei, W. (2014), "Effect of ball milling on the defeat of few-layer graphene and properties of copper matrix composites", *Acta Metallurgica Sinica*, **27**(5), 937-943. https://doi.org/10.1007/s40195-014-0156-x.

Deysher, G., Shuck, C.E., Hantanasirisakul, K., Frey, N.C., Foucher, A.C., Maleski, K., Sarycheva, A., Shenoy, V.B., Stach, E.A. and Anasori, B. (2019), "Synthesis of Mo_4VAlC_4 MAX phase and two-dimensional Mo_4VC_4 MXene with five atomic layers of transition metals", *ACS Nano*, **14**(1), 204-217. https://doi.org/10.1021/acsnano.9b07708.

Eom, W., Shin, H., Ambade, R.B., Lee, S.H., Lee, K.H., Kang, D.J. and Han, T.H. (2020), "Large-scale wet-spinning of highly electroconductive MXene fibers", *Nature Commun.*, **11**(1), 2825. https://doi.org/10.1038/s41467-020-16671-1.

Eltaher, M.A., Wagih, A., Melaibari, A., Fathy, A. and Lubineau, G. (2020), "Effect of Al_2O_3 particles on mechanical and tribological properties of Al–Mg dual-matrix nanocomposites", *Ceram. Int.*, **46**(5), 5779-5787. https://doi.org/10.1016/j.ceramint.2019.11.028.

Fehling, H. (1849), "The quantitative determination of sugar and

starch by means of copper sulfate", *Annalen der Chemie und Pharmacie*, **72**(1), 106-113. https://doi.org/10.1002/jlac.18490720112.

Feng, W., Luo, H., Wang, Y., Zeng, S., Tan, Y., Deng, L., Zhou, X., Zhang, H. and Peng, S. (2019), "MXenes derived laminated and magnetic composites with excellent microwave absorbing performance", *Scientific Reports*, **9**(1), 1-10. https://doi.org/10.1038/s41598-019-40336-9.

Halim, J., Lukatskaya, M.R., Cook, K.M., Lu, J., Smith, C.R., Näslund, L., May, S.J., Hultman, L., Gogotsi, Y. and Eklund, P. (2014), "Transparent conductive two-dimensional titanium carbide epitaxial thin films", *Chem. Mater.*, **26**(7), 2374-2381. https://doi.org/10.1021/cm500641a.

Halim, J., Persson, I., Eklund, P., Persson, P.O. and Rosen, J. (2018), "Sodium hydroxide and vacuum annealing modifications of the surface terminations of a Ti_3C_2 (MXene) epitaxial thin film", *RSC Adv.*, **8**(64), 36785-36790. https://doi.org/10.1039/C8RA07270A.

Hwang, J., Yoon, T., Jin, S.H., Lee, J., Kim, T.S., Hong, S.H. and Jeon, S. (2013), "Enhanced mechanical properties of graphene/copper nanocomposites using a molecular-level mixing process", *Adv. Mater.*, **25**(46), 6724-6729. https://doi.org/10.1002/adma.201302495.

Kim, B., Taylor, L., Troy, A., McArthur, M. and Ptaszynska, M. (2018), "The effects of Graphene Oxide flakes on the mechanical properties of cement mortar", *Adv. Nano Res.*, **21**(3), 261-267. http://doi.org/10.12989/cac.2018.21.3.261.

Kim, W.J., Lee, T.J. and Han, S. (2014), "Multi-layer graphene/copper composites: Preparation using high-ratio differential speed rolling, microstructure and mechanical properties", *Carbon*, **69**, 55-65. https://doi.org/10.1016/j.carbon.2013.11.058.

Khamaj, A., Farouk, W. M., Shewakh, W. M., Abu-Oqail, A., Wagih, A. and Abu-Okail, M. (2021), "Effect of lattice structure evolution on the thermal and mechanical properties of Cu–Al_2O_3/GNPs nanocomposites", *Ceram. Int.*, **47**(12), 16511-16520. https://doi.org/10.1016/j.ceramint.2021.02.219.

Kobayashi, Y., Nakazawa, H., Maeda, T., Yasuda, Y. and Morita, T. (2017), "Synthesis of metallic copper nanoparticles and metal-metal bonding process using them", *Adv. Nano Res.*, **5**(4), 359-372. http://doi.org/10.12989/anr.2017.5.4.359.

Li, M., Che, H., Liu, X., Liang, S. and Xie, H. (2014), "Highly enhanced mechanical properties in Cu matrix composites reinforced with graphene decorated metallic nanoparticles", *J. Mater. Sci.*, **49**(10), 3725-3731. https://doi.org/10.1007/s10853-014-8082-x.

Li, Y., Ding, L., Liang, Z., Xue, Y., Cui, H. and Tian, J. (2020), "Synergetic effect of defects rich MoS_2 and Ti_3C_2 MXene as cocatalysts for enhanced photocatalytic H_2 production activity of TiO_2", *Chem. Eng. J.*, **383** 123178. https://doi.org/10.1016/j.cej.2019.123178.

Lide, D.R. (2000), *CRC Handbook of Chemistry and Physics*, CRC Press, Florida, U.S.A.

Liu, L., Ying, G., Hu, C., Zhang, K., Ma, F., Su, L., Zhang, C. and Wang, C. (2019), "Functionalization with MXene (Ti_3C_2) enhances the wettability and shear strength of carbon fiber-epoxy composites", *ACS Appl. Nano Mater.*, **2**(9), 5553-5562. https://doi.org/10.1021/acsanm.9b01127.

Liu, L., Ying, G., Wen, D., Zhang, K., Hu, C., Zheng, Y., Zhang, C., Wang, X. and Wang, C. (2021), "Aqueous solution-processed MXene ($Ti_3C_2T_x$) for non-hydrophilic epoxy resin-based composites with enhanced mechanical and physical properties", *Mater. Des.*, **197**, 109276. https://doi.org/10.1016/j.matdes.2020.109276.

Liu, M., Wang, H., Zeng, H. and Li, C. (2015), "Silver (I) as a widely applicable, homogeneous catalyst for aerobic oxidation of aldehydes toward carboxylic acids in water–"silver mirror": From stoichiometric to catalytic", *Science Advances*, **1**(2), e1500020. https://doi.org/10.1126/sciadv.1500020.

Low, S. and Shon Y. (2018), "Molecular interactions between pre-formed metal nanoparticles and graphene families", *Adv. Nano Res.*, **6**(4), 357-375. http://doi.org/10.12989/anr.2018.6.4.357.

Naguib, M., Kurtoglu, M., Presser, V., Lu, J., Niu, J., Heon, M., Hultman, L., Gogotsi, Y. and Barsoum, M.W. (2011), "Two-dimensional nanocrystals produced by exfoliation of Ti_3AlC_2", *Adv. Mater.*, **23**(37), 4248-4253. https://doi.org/10.1002/adma.201102306.

Naguib, M., Mashtalir, O., Carle, J., Presser, V., Lu, J., Hultman, L., Gogotsi, Y. and Barsoum, M.W. (2012), "Two-dimensional transition metal carbides", ACS Nano, **6**(2), 1322-1331. https://doi.org/10.1021/nn204153h.

Naguib, M., Mashtalir, O., Lukatskaya, M.R., Dyatkin, B., Zhang, C., Presser, V., Gogotsi, Y. and Barsoum, M.W. (2014), "One-step synthesis of nanocrystalline transition metal oxides on thin sheets of disordered graphitic carbon by oxidation of MXenes", *Chem. Commun.*, **50**(56), 7420-7423. https://doi.org/10.1039/C4CC01646G.

Sadoun, A.M., Fathy, A., Abu-Oqail, A., Elmetwaly, H.T. and Wagih, A. (2020), "Structural, mechanical and tribological properties of Cu–ZrO_2/GNPs hybrid nanocomposites", *Ceram. Int.*, **46**(6), 7586-7594. https://doi.org/10.1016/j.ceramint.2019.11.258.

Sadoun, A.M., Najjar, I. and Wagih, A. (2021), "Electroless-plating of Ag nanoparticles on Al_2O_3 and graphene Nano sheets (GNs) for improved wettability and properties of Al–Al_2O_3/GNs nanocomposites", *Ceram. Int.*, **47**(8), 10855-10865. https://doi.org/10.1016/j.ceramint.2020.12.203.

Si, X., Chen, F., Deng, Q., Du, S., Huang, Q. (2018), "Preparation and property of MXene/copper alloy composites", *J. Inorg. Mater.*, **33**(6), 603-608. https://doi.org/10.15541/jim20170297.

Shah, S.A., Habib, T., Gao, H., Gao, P., Sun, W., Green, M.J. and Radovic, M. (2016), "Template-free 3D titanium carbide ($Ti_3C_2T_x$) MXene particles crumpled by capillary forces", *Chem Commun*, **53**(2), 400-403. https://doi.org/10.1039/C6CC07733A.

Shen, C., Wang, L., Zhou, A., Wang, B., Wang, X., Lian, W., Hu, Q., Qin, G. and Liu, X. (2018), "Synthesis and electrochemical properties of two-dimensional RGO/$Ti_3C_2T_x$ nanocomposites", *Nanomaterials*, **8**(2), 80. https://doi.org/10.3390/nano8020080.

Su, L., Ying, G., Liu, L., Ma, F. and Wang, C. (2018), "$Ti_3C_2T_x$ on copper and nickel foams with improved electrochemical performance produced via solution processing for supercapacitor", *Process. Appl. Ceram.*, **12**(4), 366-373. https://doi.org/10.2298/PAC1804366S.

Sun, Q., Peng, Y., Chen, H., Chang, K., Qiu, Y. and Lai, S. (2016), "Photoelectrochemical oxidation of ibuprofen via Cu_2O-doped TiO_2 nanotube arrays", *J. Hazard. Mater.*, **319**, 121-129. https://doi.org/10.1016/j.jhazmat.2016.02.078.

Wagih, A. (2015), "Mechanical properties of Al–Mg/Al_2O_3 nanocomposite powder produced by mechanical alloying", *Adv. Powder. Technol.*, **26**(1), 253-258. https://doi.org/10.1016/j.apt.2014.10.005.

Wagih, A. and Fathy, A. (2016), "Experimental investigation and FE simulation of nano-indentation on Al–Al_2O_3 nanocomposites", *Adv. Powder. Technol.*, **27**(2), 403-410. https://doi.org/10.1016/j.apt.2016.01.021.

Wagih, A., Fathy, A., Ibrahim, D., Elkady, O. and Hassan, M. (2018), "Experimental investigation on strengthening mechanisms in Al-SiC nanocomposites and 3D FE simulation of Vickers indentation", *J. Alloy. Compd.*, **752**, 137-147. https://doi.org/10.1016/j.jallcom.2018.04.167.

Wang, L., Chen, L., Song, P., Liang, C., Lu, Y., Qiu, H., Zhang, Y., Kong, J. and Gu, J. (2019), "Fabrication on the annealed $Ti_3C_2T_x$ MXene/Epoxy nanocomposites for electromagnetic interference shielding application", *Compos. Part B Eng.*, **171**,

111-118. https://doi.org/10.1016/j.compositesb.2019.04.050.
Wang, L., Cui, Y., Li, B., Yang, S., Li, R., Liu, Z., Vajtai, R. and Fei, W. (2015a), "High apparent strengthening efficiency for reduced graphene oxide in copper matrix composites produced by molecule-lever mixing and high-shear mixing", *RSC Adv*., **5**(63), 51193-51200. https://doi.org/10.1039/C5RA04782J.
Wang, L., Cui, Y., Yang, S., Li, B., Liu, Y., Dong, P., Bellah, J., Fan, G., Vajtai, R. and Fei, W. (2015b), "Microstructure and properties of carbon nanosheet/copper composites processed by particle-assisted shear exfoliation", *RSC Adv*., **5**(25), 19321-19328. https://doi.org/10.1039/C4RA14255A.
Xu, Y., Liang, D., Liu, M. and Liu, D. (2008), "Preparation and characterization of Cu_2O–TiO_2: Efficient photocatalytic degradation of methylene blue", *Mater*. *Res*. *BULL*., **43**(12), 3474-3482. https://doi.org/10.1016/j.materresbull.2008.01.026.
Ying, G., Dillon, A.D., Fafarman, A.T. and Barsoum, M.W. (2017), "Transparent, conductive solution processed spincast 2D Ti_2CT_x (MXene) films", *Mater*. *Res*. *Lett*., **5**(6), 391-398. https://doi.org/10.1080/21663831.2017.1296043.
Yu, X., Michael, N., Mochalin, V.N., Barsoum, M.W., Yury, G., Xiqian, Y., Kyung-Wan, N., Xiao-Qing, Y., Kolesnikov, A.I. and Kent, P.R.C. (2014), "Role of surface structure on Li-ion energy storage capacity of two-dimensional transition-metal carbides", *J*. *Am*. *Chem*. *Soc*., **136**(17), 6385-6394. https://doi.org/10.1021/ja501520b.
Zhang, D. and Zhan, Z. (2016a), "Experimental investigation of interfaces in graphene materials/copper composites from a new perspective", *RSC Adv*., **6**(57), 52219-52226. https://doi.org/10.1039/C6RA07606H.
Zhang, D. and Zhan, Z. (2016b), "Strengthening effect of graphene derivatives in copper matrix composites", *J*. *Alloy*. *Compd*., **654**, 226-233. https://doi.org/10.1016/j.jallcom.2015.09.013.
Zhang, H., Wang, L., Zhou, A., Shen, C., Dai, Y., Liu, F., Chen, J., Li, P. and Hu, Q. (2016), "Effects of 2-D transition metal carbide Ti_2CT_x on properties of epoxy composites", *RSC Adv*., **6**(90), 87341-87352. https://doi.org/10.1039/C6RA14560D.
Zhang, K., Ying, G., Liu, L., Wu, D., Wang, X. and Zhou, Y. (2019), "Three-dimensional porous Ti3C2Tx-NiO composite electrodes with enhanced electrochemical performance for supercapacitors", *Materials*, **12**(1), 188. https://doi.org/10.3390/ma12010188.
Zhao, C. and Wang, J. (2014), "Fabrication and tensile properties of graphene/copper composites prepared by electroless plating for structrual applications", *Physica Status Solidi* (*a*), **211**(12), 2878-2885. https://doi.org/10.1002/pssa.201431478.
Zhao, H., Lv, J., Sang, J., Zhu, L., Zheng, P., Andrew, G. and Tan, L. (2018), "A facile method to construct MXene/CuO nanocomposite with enhanced catalytic activity of CuO on thermal decomposition of Ammonium Perchlorate", *Materials*, **11**(12), 2457. https://doi.org/10.3390/ma11122457.